NASA Technical Memorandum 103737

High Temperature Performance Evaluation of a Hypersonic Engine Ceramic Wafer Seal

Bruce M. Steinetz
Lewis Research Center
Cleveland, Ohio

April 1991

NASA

HIGH TEMPERATURE PERFORMANCE EVALUATION OF A HYPERSONIC ENGINE CERAMIC WAFER SEAL

Bruce M. Steinetz
National Aeronautics and Space Administration
Lewis Research Center
Cleveland, Ohio 44135

SUMMARY

Leakage rates of an innovative hypersonic engine seal have been measured using a specially developed static high temperature seal test fixture at NASA Lewis Research Center. The 3-ft long structural panel-edge seal is designed to minimize leakage of high temperature, high pressure gases past the movable panels of advanced ramjet/scramjet engines. The seal is made of a stack of precision machined ceramic wafer pieces that are inserted into a closely conforming seal channel in the movable engine panel. The wafer seal accommodates the significant distortions in the adjacent engine walls through relative sliding between adjacent wafers.

Seal leakage rates are presented for engine simulated air temperatures up to 1350 °F and for engine pressures up to 100 psi. Leakage rates are also presented for the seal sealing both a flat wall condition, and an engine simulated distorted wall condition in which the distortion was 0.15 in. in only an 18 in. span. Seal leakage rates were low, meeting an industry-established tentative leakage limit for all combinations of temperature, pressure and wall conditions considered. Comparisons are made between the measured leakage rates and leakage rates predicted using a seal leakage model developed from externally-pressurized gas film bearing theory.

INTRODUCTION

A critical mechanical system in advanced hypersonic engines is the panel-edge seal system that seals gaps between the articulating engine panels and the stationary engine splitter walls. Extreme often conflicting demands are placed on the seal systems. The seals are required to minimize leakage of extremely high temperature (600 to over 5000 °F), high pressure (up to 100 psi) flowpath gases and must be compliant to seal against sidewalls that may be severely distorted due to the pressure and thermal loads. Further complicating the seal's challenge is the need to seal against these sidewalls as the seal and the movable engine panel are wiped across the face of the distorted sidewall.

As is described in reference 1, a family of advanced seal concepts is being developed at NASA Lewis Research Center to meet these demanding requirements. The ceramic wafer seal described in several previous papers (see refs. 1 to 4) is a leading candidate for the hypersonic engines being developed for the National Aerospace Plane (NASP). Room temperature measurements showed the wafer seal to have the lowest overall leakage amongst four seal concepts. Fabricating the seal of high temperature engineered ceramic allows the seal wafers to operate at temperatures up to 2500 °F without coolant. Thermal-structural analyses (ref. 4) performed under engine simulated temperatures, pressures, and the extreme heating rates of Mach 10 hypersonic flight have shown that the seal (made of high conductivity silicon carbide) can withstand this punishing environment, requiring only a small flow rate of helium purge coolant.

Building on this previous work, the objectives of this investigation are to: (1) demonstrate the performance of the seal and required preload techniques at engine simulated temperatures and pressures; (2) assess materials issues such as differences in coefficients of thermal expansion on leakage rates; (3) assess seal leakage rates as a function of pressure, temperature and adjacent wall condition; and to (4) develop a database of seal leakage rates to validate seal leakage modelling.

Seal leakage models are useful tools for seal designers for several reasons. Using validated seal leakage models, designers are able to estimate the percent of engine core flow leaked past the engine panels as a function of the mission profile, seal length and engine pressures and temperatures. Engine designers can use closed-form seal leakage equations in global engine performance computer codes to predict the effect of seal leakage on engine performance. Leakage models serve a second perhaps more important purpose of estimating the coolant flow rates for engine stations such as the combustor where some form of positive purge is required to cool the seal and inert backside engine cavities.

APPARATUS AND PROCEDURES

Test Set-Up

High temperature leakage measurements were made for the ceramic wafer seal using a specially developed panel-edge seal test fixture described in detail in reference 2. Three foot seal specimens were mounted in the Inconel test fixture shown in schematic in figure 1. The seal and rig were heated using a series of electric-resistance surface conduction and air heaters that could heat the rig to 1500 °F. Metered pressurized air is supplied to the base of the seal through the in-line air-heaters.

The wafer seal is mounted in a close tolerance seal channel. The channel tolerance was set at 0.004 in. larger than the wafer seal height using the adjustable "L"-shaped seal retainer shown in cross section in figure 1. The seal is preloaded against the adjacent wall representing the engine splitter wall using a series of pressurized Inconel metal bellows. Seal contact pressures up to 50 psi were examined.

On both ends of the seal, specially developed hermetically sealed axial preloaders were used to apply uniform axial loads to the seal in attempts to minimize inter-wafer leakage. The special bellows design allowed uniform preload to be applied to the seal ends without introducing end leakage paths, even though significant (up to 0.2 in. over the 3-ft. long seal) differential thermal growths were observed.

Seal Specimen

The ceramic wafer seal tested herein is shown in the movable engine panel in figure 2. The ceramic wafer seal consisted of a stack of ceramic wafers mounted in the seal channel and preloaded against the adjacent wall using the lateral metal bellows preload system described. The ceramic wafers used in these tests are made of high density aluminum oxide (Al_2O_3) ceramic. The wafers are 0.500±0.001 in. square and are 0.125±0.001 in. thick. The wafer faces are smooth (< 20 μin. RMS) and parallel to within 0.001 in. so that leakage between adjacent wafers would be

minimized. The wafer corners are rounded with a 0.06 to 0.09 in. corner radii to prevent the wafers from digging into the engine panel and to minimize wafer corner stresses. At each end of the seal (e.g., where the seal is "built-in" to the seal test fixture) special wafers with square ends were used to virtually eliminate end leakages.

Adjacent Wall Condition

A simple method of prescribing various engine wall conditions was used during these tests. A front wall or cover plate is made with two precision machined surfaces. One side is finished flat overall. Bolting this side toward the seal results in an inter-panel gap width of 0.20 in. over the full 3-ft length, (accounting for the thin ≈0.016 in. high-temperature head gasket). The opposite side has a sinusoidal wave machined onto it. The wave bulges inward toward the seal with a peak of 0.15 in. at the center (see fig. 1). When bolted against the seal, the inter-panel gap width is 0.05 in. at the center sinusoidally increasing to the full 0.20 in. at both ends. The flow area for the straight gap condition is 7.2 $in.^2$. The flow area for the wavy wall condition is 4.5 $in.^2$.

Procedure

Leakage rates were measured for the seal for each wall condition at four temperatures from room temperature to 1350 °F. For each wall condition and each temperature, the engine simulated pressure was varied typically from 100 psi down to 10 psi and then back up to 100 psi for at least one complete pressure cycle. In several cases the seal leakage rates were measured for multiple pressure cycles to establish seal leakage repeatability.

Prior to heating to temperature, the wafers were first preset to the preferred sealing position (e.g., in contact with the front wall and in contact with the top of the seal channel) using the lateral preload (≈50 psi seal contact pressure) and the engine pressure. The wafers were axially compressed with 10 lb (or 40 psi contact pressure for the 0.5 in. square seal) using both left and right axial preloaders.

Instrumentation

As discussed in detail in reference 2, leakage measurements were made using a heated capillary-tube calibrated flow meter with accuracy better than 1 percent. Pressure measurements were made upstream of the seal using a series of capacitance pressure transducers with better than 0.5 percent accuracy. Gage pressure measurements were made since the seal leakage was exhausted to ambient conditions. Air temperature measurements were made using micro-gage open-bead thermocouples inserted in the flow just upstream of the seal. Lateral preload was measured by measuring pressure in the manifold supplying pressure to the lateral bellows. Axial preloads were measured using calibrated load cells mounted in series with the axial preload system.

RESULTS AND DISCUSSION

Experimental Results

Pressure and temperature effects. - The ceramic wafer leakage rates were measured over the anticipated engine pressure loads at several engine simulated temperatures. Leakage rates for the seal sealing against the flat wall conditions are shown in figure 3 at air temperatures of 73, 200, 940, and 1350 °F. The low to moderate temperatures correspond to engine inlet temperatures under high speed flight conditions. The high temperature gas corresponds to engine gas temperatures 1- to 2-ft forward of the engine combustion chamber at a Mach 8 flight condition.

The seal leakage rates for each of the temperatures examined were below the industry-established tentative leakage limit of 0.004 lb/s-ft. (see ref. 1) shown as the dashed horizontal line for reference purposes in each of the figures. Leakage rates generally decreased with increasing temperature up to moderate temperatures at which point the trend reversed and a slight increase in leakage rates was observed. A potential explanation for this leakage temperature-dependence is given below where the measured and predicted leakage rates are compared.

Adjacent wall effects. - The leakage rates for the seal sealing against an engine simulated distorted wall condition are shown in figure 4 as a function of engine pressure and at engine simulated temperatures of 76, 530, 1000, and 1350 °F. Similar to the trends found when sealing against the flat wall, the leakage rates decrease with increasing temperature up to 1000 °F. Then for intermediate to high temperatures the seal leakage rates increase with increasing temperature.

Comparing the leakage rates for the two wall conditions examined, the leakage rates for the seal sealing against the flat wall are slightly more than those measured sealing against the distorted wall condition, as is shown in figure 5 for an applied pressure differential of 100 psi. The reason for this observed trend can be understood from the total effective area the seal is sealing in both wall conditions. Because the distorted wall pushes in against the seal the total effective area to be sealed is only 4.5 $in.^2$ versus 7.2 $in.^2$ for the uniform or flat wall condition.

The seal performed well through the sequence of tests described. The ceramic wafer seal met the tentative leakage limit for all combinations of applied engine pressure differentials, temperatures, and simulated wall conditions. It is emphasized to achieve these performance results certain important conditions must be met.

Precision machined wafers must be used to ensure intimate contact with their neighbors and with adjacent sealing surfaces. The need for precision machined surfaces was demonstrated by a test at room temperature in which one wafer with poor wafer-face parallelism was accidentally installed. Leakage rates for this seal build were up to 20 percent higher than those shown herein. It is also emphasized that the seal achieves the performance results shown when in its preferred sealing position against the top channel surface and against the adjacent wall.

Theoretical Results

A closed form seal leakage flow model has been developed to predict seal leakage response over the wide range of engine pressures and temperatures. The leakage model

is based on externally pressurized gas film bearing theory modified to account for the special features of the seal. Details of the model development are given in the appendix section of this paper. The important results obtained in the appendix are summarized next.

Leakage pressure-dependence. - The compressible nature of the gas for the high 7.8:1 pressure ratios found in the seal results in a leakage flow rate expression dependent on the difference in the squares of the supply and exhaust pressure, (e.g., a parabolic pressure dependence). The measured leakage rates though slightly parabolic in nature are less so than predicted by the unmodified constant film-height gas-film bearing theory.

The constant film-height leakage flow equation over-predicts the measured seal leakage by a considerable margin (≈53 percent), at the highest pressure differential of 100 psi. As demonstrated in the appendix the cause of this discrepancy lies in the constant film-height assumption. As the applied engine pressure increases considerable forces develop to reduce the film-heights between the seal wafers and the adjacent sealing surfaces. Modifying the flow equations to allow for variable film-height as a function of applied pressure differential allows a close prediction within 6 percent of the measured leakage rates even for the highest pressure differential of 100 psi.

The seal leakage rate per unit length developed in the appendix is shown in equation 1:

$$\dot{m}/L = \frac{(P_s^2 - P_o^2)}{24\mu RT}\left(\frac{h^3_{1,v}}{H_1} + \frac{h^3_{2,v}}{H_2} + \frac{Ngh^3_{CTE}}{LH_2}\right) \qquad (1)$$

There are three potential seal leakage paths: (1) between the wafer and the top surface of the seal channel accounted for by the $h_{1,v}$ term; (2) between the seal nose and the adjacent wall accounted for by the $h_{2,v}$ term; and (3) at high temperatures through the inter-wafer gaps caused by differential seal and engine panel thermal expansion, accounted for by the h_{CTE} term. The other variables in the model describe the seal's length, L; height H_2; contact dimension with the top channel H_1; inter-panel gap width, g; and number of wafer interfaces N, as described in the appendix. The leading coefficient includes terms for the gas properties, gas temperature, and pressure differential applied across the seal.

Leakage temperature-dependence. - The leakage flow equation has been used to predict the leakage as a function of pressure. The results of these calculations are shown in figures 6, 7, and 8 along with the measured results. In each of these curves the measured results are shown with a solid line and the predictions made using the equation are shown with the dashed line. As is well known, gas viscosity increases with temperature. Throughout these analyses the power law of gas viscosity: $\mu = \mu_o(T/T_o)^{2/3}$ (ref. 5) was used for the air viscosity in equation 1.

In figure 6, the measured and predicted leakage rates are compared for a fixed engine pressure differential of 20 psi. The correlation between the predicted and measured leakage rates is very good for the full temperature range. In figure 7 the measured and predicted leakage rates are compared for a fixed engine pressure differential of 40 psi. The correlation between the predicted and measured leakage rates is reasonable for this pressure differential. The maximum discrepancy between the measured and predicted was slightly over 20 percent and occurred at intermediate

temperatures of about 500 °F. This discrepancy narrowed to about 14 percent at gas temperatures of 1350 °F.

Comparisons are made between the measured and predicted leakage rates at the maximum expected pressure differential of 100 psi in figure 8. Examining figure 8, it is noted that both the measured trends of decreasing leakage followed by slightly increasing leakage rates are modeled by equation 1. For this pressure case the maximum discrepancy between the predicted and measured is about 38 percent at 500 °F. However, at 1350 °F the discrepancy between measured and predicted was only 18 percent.

Discrepancies as noted above can be caused by several sources. The most probable cause is thermally-induced nonuniform changes in the size and shape of the film-heights (h_i). Since the flow responds to changes in gap height cubed one can see why thermally induced changes in contact condition can lead to a appreciable changes in leakage. As an example, analytically changing gap height by 11 percent results in a 38 percent change in leakage. This observation underscores the need to maintain small gaps through optimal loading, wafer design, and tolerances.

It is noted that even though some modeling discrepancies are observed the absolute magnitude of the leakage rates are still below the industry-established tentative leakage limit, shown by the horizontal dashed line in the figures.

Gas property dependence. - Throughout the engine the seal will be required to seal a variety of gases and gas mixtures. Furthermore it is contemplated to use the seal in two different sealing approaches in the engine. In areas such as the engine inlet where the ambient flow temperatures are below the seal operating temperature and where hydrogen is not present, the seal can be used in the traditional manner of minimizing parasitic core flow losses past the movable engine panels.

In the engine combustion area, the seal designer's paramount concern is to prevent the leakage of the extremely hot flow path gases containing unburned mixtures of hydrogen-oxygen from leaking behind the movable engine panels. Leakage of these potentially explosive gases could cause destruction to or loss of the engine. In these critical areas it is contemplated to use a dual seal approach in which the cavity between the two seals is pressurized with an inert gas purge nominally 10 to 15 psi above the ambient engine core pressure. In this approach the seal functions to limit the purge gas flow into the engine combustion chamber minimizing loss of coolant which is at a premium. The two key advantages of this approach are that the purge gas inerts the cavity between the parallel seals precluding leakage of hydrogen gases and the purge gas cools the seals. The study conducted in reference 4 demonstrated that using a minimal purge flow of 70 °F helium the seal could be kept below it operating temperature for a near maximum engine heating rate of 1160 Btu/ft^2 sec.

A variety of gases including helium and nitrogen have been considered to serve the dual role of inerting the central cavity and cooling the seals. Helium is a prime candidate because of its low density and good cooling effectiveness (e.g., heat capacity). Equation 1 can be used to estimate the relative flow rates of various gases for similar pressure, temperature and gap conditions. The gas properties are modelled in equation 1 by the viscosity, μ, and gas constant, R. An expression for the relative flow rates of two gases (e.g., A and B) can be found by taking the ratio of these gas properties and using the relation that the gas constant R is simply the universal gas constant R* divided by the gas's molecular weight, MW:

$$\frac{(\dot{m}/L)_A}{(\dot{m}/L)_B} = \frac{MW_A}{MW_B}\,\frac{\mu_B}{\mu_A} \qquad (2)$$

The above expression can be used to estimate the relative leakage rate of helium, for instance, relative to the air leakage rates measured herein. Substituting values for both gas's molecular weights and viscosities at room temperature (ref. 5) we note that for other things held constant the helium leakage rate would be 0.126 (or approximately 1/8th) that of the air leakage rates measured herein:

$$\frac{(\dot{m}/L)_{He}}{(\dot{m}/L)_{Air}} = \frac{4}{29}\,\frac{1.22x10^{-5}}{1.34x10^{-5}} = 0.126 \qquad (3)$$

Wafer size effects. - The half-inch wafer selected for this study was suitable for the space available along the edge of the panels being considered for the engine. It is observed from equation 1 that increasing the contact dimensions H_1 and H_2 between the seal and adjacent surfaces can have a beneficial effect on seal leakage. Increasing the wafer size and making either a large square wafer or a rectangular wafer would according to equation (1) linearly decrease the seal leakage rates.

Using rectangular instead of square wafers offers the added benefit of improving the wafers "piloting" ability within the seal channel by increasing the seal wafers length-to-height ratio. Both of these benefits however must be optimized within seal weight and space limitations established by the overall engine design.

SUMMARY AND CONCLUSIONS

Leakage rates of a high temperature flexible ceramic wafer seal have been assessed using a specially designed static high temperature panel-edge seal fixture. The seal is designed to seal the many feet of linear gaps between movable structural panels and adjacent splitter walls of advanced hypersonic ramjet/scramjet engines. The seal is made of precision machined wafers mounted in a closely conforming seal channel machined in the movable engine panel. The seal derives its flexibility to accommodate the large distortions in the counterface adjacent engine panels through relative sliding of adjacent wafers. The seal is preloaded from behind using a series of high temperature Inconel bellows that maintain the seal in contact with the adjacent wall.

Typical of the engine, 3-ft lengths of the seal were tested under simulated pressure differentials, temperatures and wall conditions. The seal was tested at pressures ranging from 10 to 100 psi and at temperatures from room temperature to 1350 °F. The seal's ability to accommodate simulated engine wall and gap conditions was measured using two wall configurations. For the flat wall condition the seal sealed a uniform 0.20 in. inter-panel gap (e.g., the space between the horizontal and vertical engine panels). For the distorted wall condition the seal sealed an engine simulated gap in which the inter-panel gap varied sinusoidally from 0.05 in. at the center increasing to the full 0.20 in. at both left and right ends.

A seal leakage flow model was developed based on Reynolds equation and externally pressurized gas film bearing theory. The leakage model allows designers to estimate seal leakage response under various gas, pressure, and temperature conditions. The model can also be used to estimate the effects of seal size on seal leakage rates.

Seal leakage is very sensitive to variations in film height between the seal and mating seal surfaces varying with film height cubed. Discrepancies were noted between the predicted and measured leakage rates as a function of pressure drop when assuming a constant film-height between the seal and the adjacent sealing surfaces. Introducing a variable (e.g., decreasing) film height with increasing pressure differential corrected the noted discrepancy at room temperature.

The seal model accounts for the three potential leakage flow paths. Two of the paths are between the seal nose and adjacent engine panel and between the seal and the downstream (e.g., top) surface of the seal channel. The third path observed at temperature is between the wafers through small gaps that open between wafers caused by a mismatch in thermal expansion coefficients between the ceramic wafer seal and the metal simulated engine-panel.

A force balance performed on the ceramic wafer seal demonstrated that the engine pressure exerts self-seating forces on the seal urging the seal toward the desired seal location. The force urging the seal against the adjacent engine sidewall is caused by the difference in the engine pressure exerted on the back of the seal and the parabolically decreasing pressure profile existing on the seal nose. The force urging the seal against the downstream surface of the seal channel is caused by the differences in the engine pressure exerted on the upstream side of the seal and the composite: ambient pressure and the parabolically decreasing pressure between the seal and the seal channel.

On the basis of these findings, the following results were obtained:

1. The ceramic wafer seal leakage rates were below the 0.004 lb/s-ft industry established tentative leakage limit for air pressure differentials up to 100 psi and temperatures up to 1350 °F. The seal leakage rates were below the leakage limit for both the flat wall condition (sealing a uniform 0.20 in. inter-panel gap) and for the engine simulated distorted wall condition (sealing a significant peak-to-peak wall distortion of 0.15 in. in only an 18 in. span).

2. Seal leakage mass flow rates decrease with increasing temperature for low to intermediate temperature (e.g., 1000 °F) as increasing gas viscosity limits flow through the small seal gaps. For temperatures above 1000 °F a small increase in the seal leakage mass flow rate is observed and is attributed to small inter-wafer gaps opening due to a mismatch in thermal expansion between the ceramic wafers and the metal simulated engine-panel.

3. Based on the seal leakage model developed, the leakage mass flow rates for gases other than the air tested can be estimated from the air data collected herein. The leakage mass flow rate of the second gas can be scaled from the air data by multiplying the measured air flow by the ratio of the second gas's molecular weight to that of air and by the ratio of the viscosity of air to the viscosity of the second gas.

Appendix - LEAKAGE MODEL FOR CERAMIC WAFER SEAL

Nomenclature:

$\dot{m}/L$	seal mass flow per unit length
P	pressure, abs.
T	temperature, abs.
g	inter-panel gap width
H_1, H_2	seal-to-wall contact dimensions
h_1, h_2	seal film heights
R	gas constant
n	polytropic exponent
c_p, c_v	heat capacities
U	seal velocity (≈ 0)
u	leakage gas velocity profile
t	time
A, B	constants
L	seal length
s, w	distance measurements as defined in Fig. 9
N	number of wafer interfaces
F	force
M	moment
x, y	coordinate directions

Greek:

α	coefficient of thermal expansion
ρ	gas density
μ	gas viscosity
μ_o	gas viscosity at room temperature

Subscripts:

1,2	seal top and seal nose surfaces
s	supply
o	exhaust
eff	effective
CTE	coefficient of thermal expansion
v	variable film height

Model Development

An analytical expression is developed herein to estimate the leakage rates of the ceramic wafer seal. The model is developed based on externally pressurized linear gas-film bearing theory. Similarities between the flow past the seal and through gas-film bearings include similar pressure ratios (8:1), geometry, and low Reynolds number flow, as will be demonstrated herein. Using Reynolds equation as a starting

point the leakage flow model is developed with some modifications required to account for some subtleties of the seal. The necessary flow variables and geometry terms used throughout this derivation are shown graphically in figure 9.

During room temperature tests two leakage paths were identified for the wafer seal, between the nose of the seal and the adjacent engine splitter wall (denoted by h_2) and between the top of the wafers and the adjacent top surface of the seal channel (denoted by h_1). The method used to identify these leakage paths was carefully placing small amounts of soap solution at each of these interfaces and examining the origins of the bubbles. Referring to figure 9 these leakage paths are shown enlarged for clarity. As will be demonstrated below these leakage were small and were <0.001 in. in size.

Pressure measurements indicated that the pressure in the cavity behind the seal wafers is equal to the supply pressure P_s, since the wafers are actually lifted out of contact with the lower surface of the seal channel. Thus the driving potential for both of the leakage paths mentioned is the engine supply pressure, P_s. Therefore the seal leakage mass flow rate is simply the sum of these two parallel leakage paths:

$$\dot{m}/L = \dot{m}_1/L + \dot{m}_2/L \tag{A1}$$

Expressions for each of these components of the mass flow rate are derived from the basic Reynolds flow equation (ref. 6) where the flow is assumed to be laminar (e.g., where the fluid inertia is neglected because of the low flow speeds):

$$\frac{\partial}{\partial x}\left(\rho h^3 \frac{\partial P}{\partial x}\right) + \frac{\partial}{\partial y}\left(\rho h^3 \frac{\partial P}{\partial y}\right) = 6\mu U \frac{\partial}{\partial x}(\rho h) + 12\mu \frac{\partial(\rho h)}{\partial t} \tag{A2}$$

The first term on the right side can be dropped since there is no high speed relative motion ($U = 0$) between the seal and the adjacent wall. For reference purposes the seal will be moved across the wall at speeds less than 1 in./sec which is not sufficient to generate a film between the seal and the wall. The transient term is dropped since only the steady-state solution is desired. The side-flow term ($\partial P/\partial y$) is also dropped since the seal is long in relation to the effective gaps.

Solution of the remaining differential equation requires a relation between the density and the pressure. For generality the polytropic expression is assumed:

$$\left(\frac{\rho}{\rho_o}\right)^n = \frac{P}{P_o} \tag{A3}$$

where n is the polytropic exponent. The two limiting cases for this expression are obtained with $n = 1$ for the isothermal flow assumption (e.g., $\partial T/\partial x = 0$) and $n = c_p/c_v$ for the adiabatic flow assumption (e.g., n equals 1.4 for air).

As others have found (refs. 6 to 8) the gas flow can be treated isothermally. Any difference in temperature between the gas and adjacent surfaces is quickly eliminated because of three important factors: (1) the thermal mass of the gas is small relative to that of the adjacent surfaces; (2) the thin film allows heat to conduct quickly through the film; and (3) the flow velocity is small so the

temperature difference is eliminated near the seal inlet. Hence for practical cases the isothermal flow assumption (n = 1.0) is valid. For flow through these small gaps, the gas temperature in these analysis is taken as the average bulk wall and seal temperature. Following the isothermal assumption the compressibility expression relating density and pressure is the ideal gas law:

$$P = \rho RT \tag{A4}$$

Substituting this expression into the simplified equation (A2) results in the following differential equation to be solved for the pressure distribution:

$$\frac{\partial}{\partial x}\left(Ph^3 \frac{\partial P}{\partial x}\right) = 0 \tag{A5}$$

The above equation can be further simplified since the film height is assumed constant across the wafer surface (e.g., $\partial h/\partial x = 0$), and by noting:

$$\frac{1}{2}\frac{\partial^2 P^2}{\partial x^2} = \frac{\partial}{\partial x}\left(P\frac{\partial P}{\partial x}\right) \tag{A6}$$

Following the above derivations, the following simplified differential equation results:

$$\frac{\partial^2 P^2}{\partial x^2} = 0 \tag{A7}$$

Solving this equation results in equations for pressure as a function of x for the region upstream of the seal and in narrow gap between the seal and the adjacent wall:

$$P^2 = \begin{cases} P_s^2 - Ax & \textit{Upstream of seal} \\ P_o^2 + B(w - x) & \textit{Through film gap} \end{cases} \tag{A8}$$

(Note: For simplicity the following derivation is for the interface between the wafer nose and the adjacent wall. The final equations developed can be modified for the interface between the seal top and seal channel by simply interchanging the required length scales as defined in fig. 9).

The two constants A and B are determined by matching the pressure and mass flow rate across the seal step:

$$A = \frac{1}{g^3}\left[\frac{P_s^2 - P_o^2}{\left(\frac{s}{g^3}\right) + \left(\frac{H_2}{h_2^3}\right)}\right] \tag{A9}$$

$$B = \frac{1}{h_2^3}\left[\frac{P_s^2 - P_o^2}{\left(\frac{s}{g^3}\right) + \left(\frac{H_2}{h_2^3}\right)}\right] \tag{A10}$$

The unit mass flow through the small gap separating the seal and the adjacent wall is found by integrating the velocity profile over the film height h:

$$\dot{m}/L = \int_0^h \rho u dy \tag{A11}$$

The laminar velocity profile u is parabolic and using the nonslip conditions along the seal (e.g., $u = 0$ at $y = 0$) and at the wall (e.g., $u = 0$ at $y = h$) yields:

$$u = \frac{-y(h-y)}{2\mu}\frac{\partial P}{\partial x} \tag{A12}$$

Substituting the velocity distribution into the mass flow equation and integrating yields:

$$\dot{m}/L = \frac{-h^3\rho}{12\mu}\frac{\partial P}{\partial x} \tag{A13}$$

Substituting the ideal gas law relation for density and noting that:

$$2P\frac{\partial P}{\partial x} = \frac{\partial P^2}{\partial x} \tag{A14}$$

results in:

$$\dot{m}/L = \frac{-h^3}{24\mu RT}\frac{\partial P^2}{\partial x} \tag{A15}$$

Differentiating equation (A8) with respect to x in the region between the seal nose and adjacent wall and substituting the results into equation (A15) gives:

$$\dot{m}_2/L = \frac{h_2^3}{24\mu RT}\frac{P_s^2 - P_o^2}{\left(\left(\frac{h_2}{g}\right)^3 s + H_2\right)} \tag{A16}$$

Examining the ratio h_2/g in the denominator for dimensions typical of the seal one finds that this term for all practical purposes can be ignored. For dimensions typical of the current investigation the ratio of the film thickness (h_2) to the inter-panel gap width (g) is only 0.004. Cubing this small number essentially removes this term from the denominator, since s and H_2 are of the same magnitudes.

Simplifying the above expression results in the basic leakage flow equation for flow (m_2/L) between the seal nose and the adjacent wall. A similar derivation can be

done for flow ($\dot{m}_1/L$) through the interface between the top of the seal and the top of the seal channel. Substituting the results of these derivations into equation (A1) yields:

$$\dot{m}/L = \frac{(P_s^2-P_o^2)}{24\mu RT}\left(\frac{h_1^3}{H_1} + \frac{h_2^3}{H_2}\right) \qquad \text{(A17)}$$

Check of assumptions. - The assumptions made in applying this theory to the seal leakage were: that the flow was laminar (e.g., Reynolds number < 500); that the seal was long (e.g., $L >> h_i$); and that the seal was smooth in relation to the seal gap height (e.g., wafer roughness < h_i). These assumptions are now checked using measured maximum flow conditions. For the seal at maximum pressure differential of 100 psi:

$\dot{m}/L$	0.004 lb_m/s ft
L	3 ft
μ	1.22 x 10^{-5} lb_m/s ft
R_{air}	53 lb ft/lb_m °R
T	76 °F
H_1	0.025 ft (0.3 in.)
H_2	0.0417 ft (0.5 in.)
P_s	114.7 psi
P_o	14.7 psi

The Reynolds number for either of the parallel paths can be written in know quantities as:

$$Re = \frac{\dot{m}_i/L}{\mu} = 160 \qquad \text{(A18)}$$

Since Re is less than 500 the flow is within the laminar regime. Rearranging the basic mass flow rate equations yields an estimate of the effective seal gap height where again it is assumed the two leakage gap heights are equal:

$$h_{eff} = \sqrt[3]{\frac{24\mu RT\,\dot{m}/L}{(P_s^2 - P_o^2)}\left(\frac{H_1H_2}{H_1 + H_2}\right)} = 0.000039\ ft = 0.00047\ in. \qquad \text{(A19)}$$

Since the seal length is much greater than the effective gap height, the second assumption is satisfied. Also the effective seal gap is greater than the roughness of the smooth (32 μin.) wafer surfaces.

Leakage Pressure-Dependence

According to the flow equation (A17) the leakage flow rate varies with the difference in the squares of the pressure. Plotting the seal leakage rates predicted by the above relation results in the parabolic leakage rate curve shown in figure 10. Also plotted in the figure is the measured room temperature leakage rate. For this case the film thicknesses h_1 and h_2 used in the model were assumed equal and

back-calculated from equation (A9) using the leakage rate measured at an applied pressure differential of 40 psi.

Good correlation between the measured and predicted leakage rates was observed for pressure differentials less than 50 psi. However the leakage model over predicts the measured leakage rates by 53 percent, at pressure differentials of 100 psi.

The likely cause of the discrepancy is the film heights h_i are not constant but are actually reduced in size as the pressure differential applied across the seal is increased. Figure 11 depicts the forces leading to smaller film thickness as the pressure differential is increased. The pressure profiles along the nose and along the top of the seal are parabolic (as shown in eq. (A8)) and are lower in magnitude than the engine supply pressure P_s exerted along the back and bottom surfaces of the seal. A force balance in each of these two directions provides expressions for the pressure induced contact forces. The resultant forces per unit length in the vertical and horizontal directions for the maximum applied pressure differential of 100 psi are 31 lb/in. and 18 lb/in., respectively. These forces combined with the counter-clockwise moment act to preload the seal wafer against its mating surfaces leading to smaller effective film thicknesses.

Using equation (19) effective film heights were calculated as a function of pressure drop across the seal. As is shown in figure 12 the film height decreases nearly linearly with increasing pressure differential. A least squares regression analysis performed resulted in a strong (correlation coefficient of $R^2 = 0.98$) correlation for a straight line fit through the data points.
The resulting linear equation is:

$$h_{1,v} = h_{2,v} = 4.95x10^{-5} - 1.131x10^{-7}(P_s - P_o) \qquad \begin{matrix} h_{i,v} = ft \\ P_s\ ,\ P_o = lb/sq.inch \end{matrix} \qquad \text{(A20)}$$

Implementing this variable film thickness into equation (A17) one can recalculate mass flow versus pressure drop. The resulting predicted leakage rates are shown in figure 13. The agreement between measured and predicted leakage rates is very good. The maximum observed discrepancy is only 6 percent at the full 100 psi pressure differential, a significant improvement over the 53 percent discrepancy observed with the fixed film height assumption.

Leakage Temperature-Dependence

The measured leakage rates are plotted versus temperature in figure 14 for a fixed pressure differential of 40 psi. Several trends are noted in this curve. For low to moderate temperatures the leakage rates decrease with increasing temperature. At intermediate temperatures the leakage rates are constant with temperature. Between moderate to high temperatures the leakage rates begin to increase slightly.

A careful examination of the properties of the seal reveals why the leakage rates do not continue to decrease with temperature as suggested by the basic leakage equation (A17).

Thermal expansion differences. - The coefficient of thermal expansion (CTE) of the aluminum-oxide wafers used in these investigations is nominally half the CTE of

the test rig made of engine simulated material (e.g., Inconel). As the 3-ft rig heats up it axially expands more than the ceramic wafers. During tests it was observed that axial preload applied by the axial preload systems was unable to maintain the wafer faces in contact, except at the extreme ends of the seal. The resisting friction forces were generated by the high engine pressures combined with the high friction coefficient of the aluminum oxide ceramic. (Note: Clearly, reduced ceramic fiction coefficients possible with advanced solid lubrication techniques under development should improve preload and hence seal leakage performance.) Therefore at the maximum temperature of 1350 °F the differential axial expansion between the wafers and the rig was 0.23 in. Uniformly dividing this differential expansion over the 288 wafers 1/8-in. thick) results in an inter-wafer gap of 0.00079 in. This inter-wafer gap is of the same order of magnitude as the film-heights calculated between the seal and the adjacent wall surfaces, and must be accounted for in the model.

Flow between wafers similar to flow around the wafers can be modelled using the externally pressurized gas film bearing theory.

Flow between wafers represents a third parallel leakage path which can be added to the basic leakage flow equation (A17) resulting in:

$$\dot{m}/L = \frac{(P_s^2 - P_o^2)}{24\mu RT}\left(\frac{h^3_{1,v}}{H_1} + \frac{h^3_{2,v}}{H_2} + \frac{Ngh^3_{CTE}}{LH_2}\right) \tag{A21}$$

In this equation the effective inter-wafer spacing is found from:

$$h_{CTE} = (\alpha_{engine\ panel} - \alpha_{wafers})\frac{L\Delta T}{N} \tag{A22}$$

where N is the number of wafer interfaces (e.g., the number of wafers minus 1), L is the seal length and ΔT is the temperature rise. The film thickness $h_{1,v}$ and $h_{2,v}$ are subscripted with a "v" to denote variable film thickness as a function of applied pressure in accordance with equation (A20.) The term g in equation (A21) is the inter-panel gap width as indicated in figure 9. Comparisons are made between the leakage rates predicted from equation (A21) and measured leakage rates in the Results and Discussion section of this paper.

REFERENCES

1. Steinetz, B.M.; DellaCorte, C.; and Sirocky, P.J.: On The Development of Hypersonic Engine Seals. NASA TP-2854, December 1988.

2. Steinetz, B.M.: A Test Fixture for Measuring High-Temperature Hypersonic Engine Seal Performance. NASA TM-103658, December 1990.

3. Steinetz, B.M.; DellaCorte, C.; and Tong, M.: Seal Concept and Material Performance Evaluation for the NASP Engine. NASA CP-7045, Vol. VI, Structures, 1989, pp 39-58.

4. Tong, M., and Steinetz, B.M.: Thermal and Structural Assessments of a Ceramic Wafer Seal in a Hypersonic Engine. NASA TM-103651, December 1990.

5. White, F.: Fluid Mechanics. McGraw Hill Book Co., 1979.

6. Ausman, J.S.: Gas Lubricated Bearings, Advanced Bearing Technology. NASA SP-38, E.E. Bisson and W.J. Anderson, eds., 1964, pp. 109-138.

7. Constantinescu, V.N.: Gas Lubrication. American Society of Mechanical Engineers, New York, 1969.

8. Licht, L.: Extension of the Conducting Sheet Analogy to Externally Pressurized Gas-Bearings. J. Basic Eng., Vol. 83, June 1961, pp. 209-212.

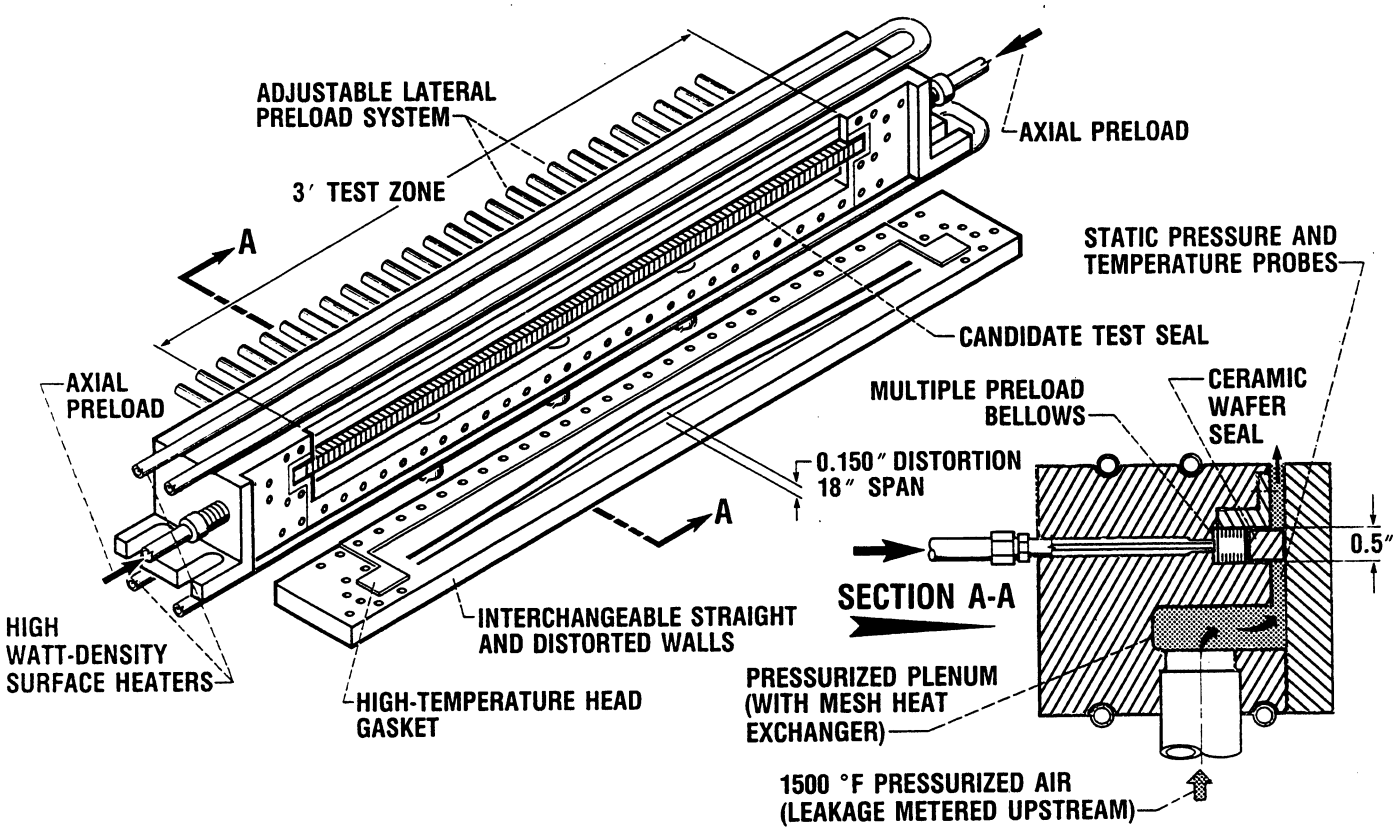

Figure 1.—Schematic of high temperature panel-edge seal test fixture.

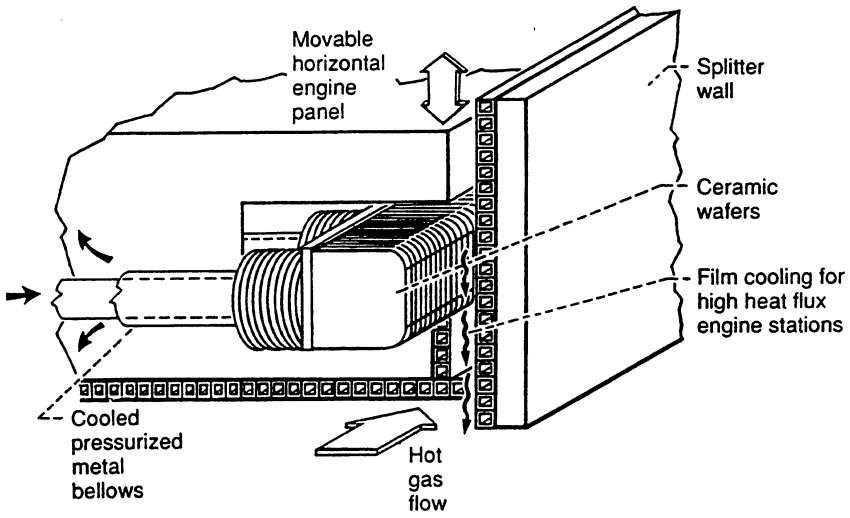

Figure 2.—Isometric of ceramic wafer seal installed in the movable engine panel.

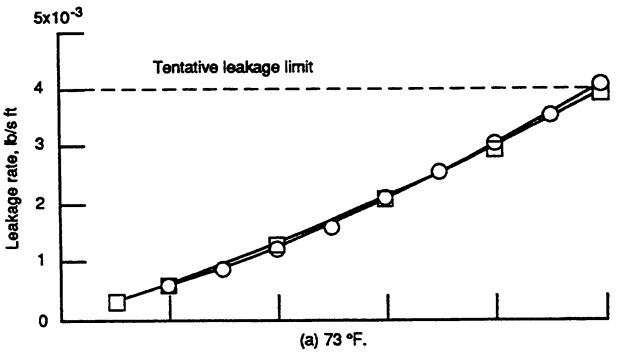

(a) 73 °F.

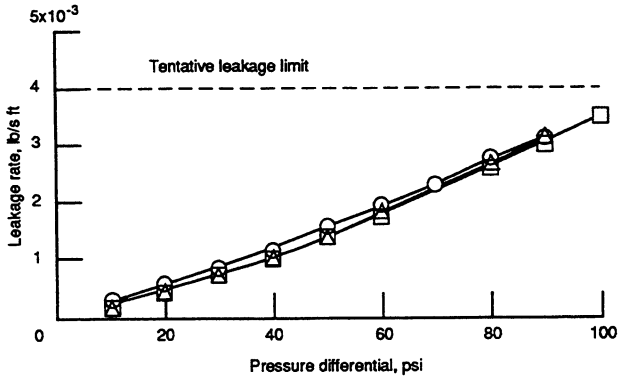

(b) 200 °F.

Figure 3.—Measured seal leakage rates versus simulated engine pressure differential sealing against the flat wall condition.

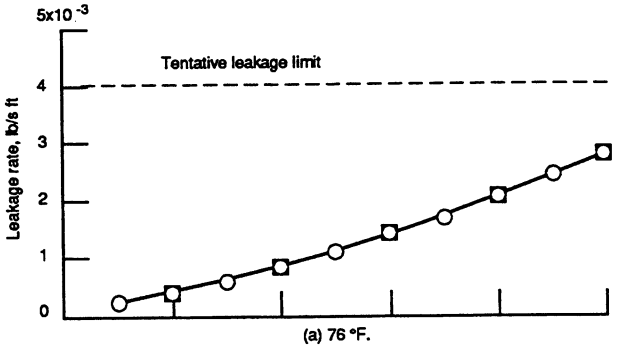

(a) 76 °F.

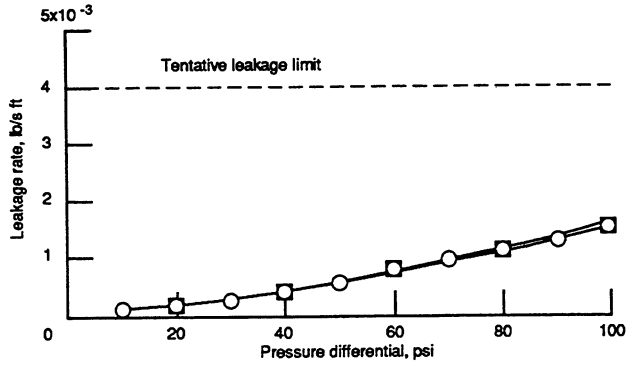

(b) 530 °F.

Figure 4.—Measured seal leakage rates versus simulated engine pressure differential sealing against the distorted wall condition.

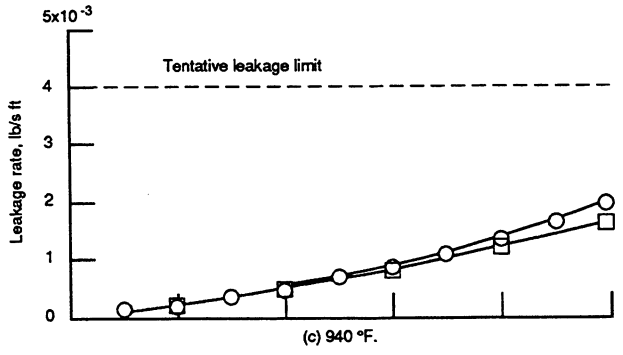

(c) 940 °F.

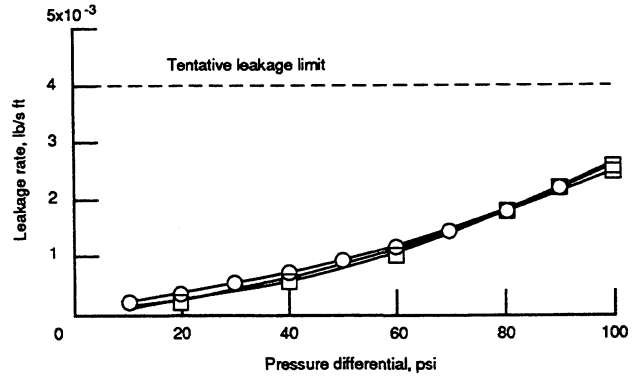

(d) 1350 °F.

Figure 3. - Concluded.

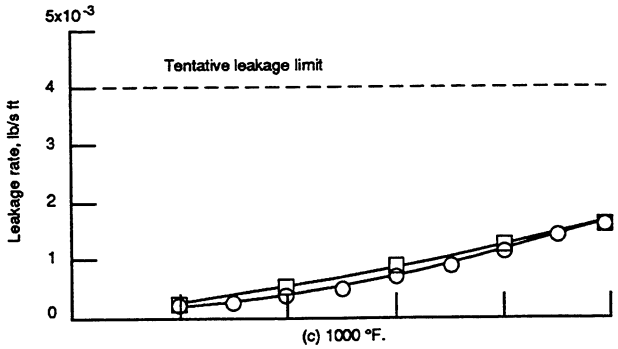

(c) 1000 °F.

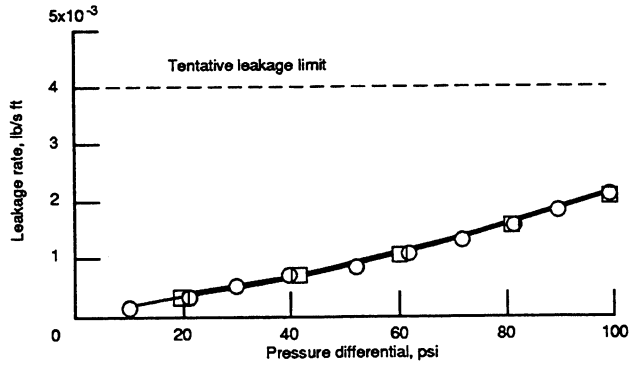

(d) 1350 °F.

Figure 4. - Concluded.

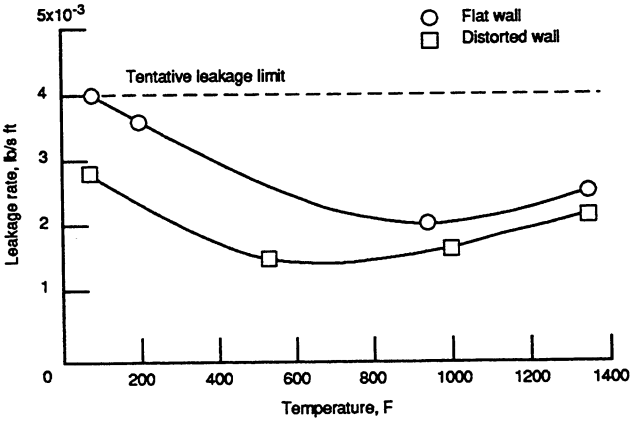

Figure 5.—Measured leakage rates versus temperature for flat and distorted wall conditions at a simulated engine pressure differential of 100 psi.

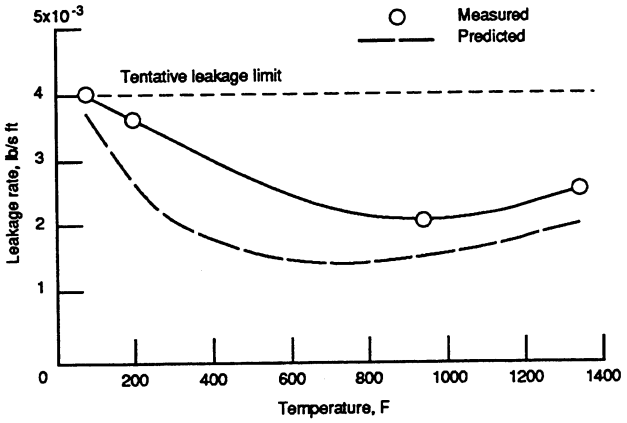

Figure 8.—Comparison of measured and predicted leakage rates as a function of temperature for a fixed engine pressure differential of 100 psi.

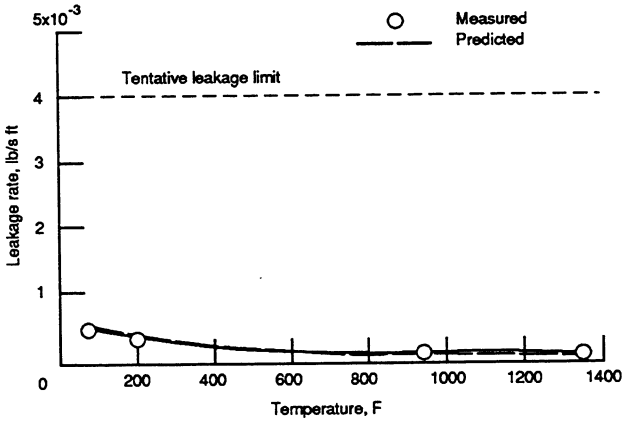

Figure 6.—Comparison of measured and predicted leakage rates as a function of temperature for a fixed engine pressure differential of 20 psi.

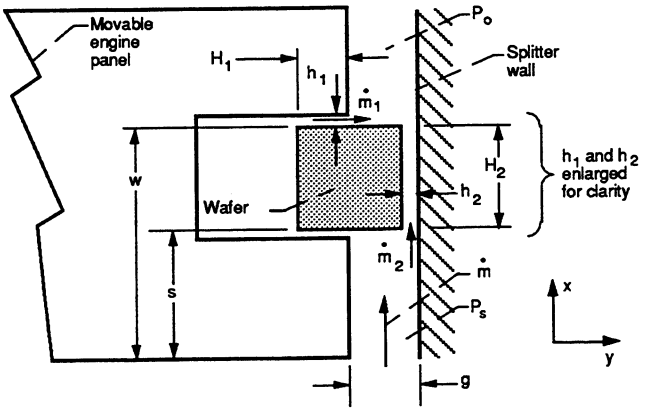

Figure 9.—Ceramic wafer seal flow model variables.

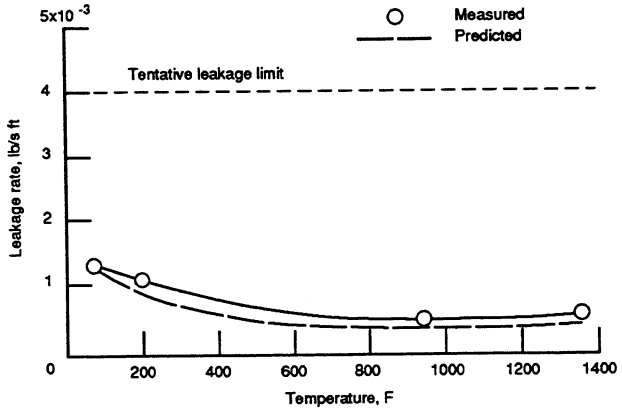

Figure 7.—Comparison of measured and predicted leakage rates as a function of temperature for a fixed engine pressure differential of 40 psi.

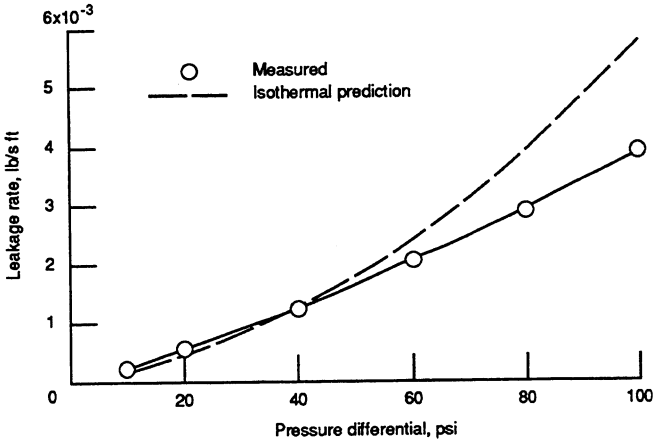

Figure 10.—Comparison of measured and predicted leakage rates versus simulated engine pressure differential using fixed film height assumption.

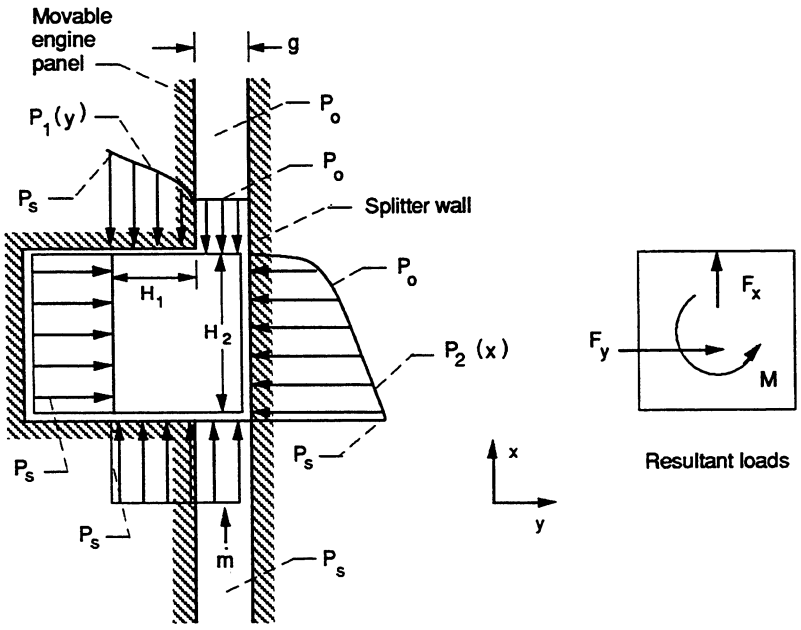

Pressure distribution

$$\Sigma\frac{F_y}{L} = \frac{F_y}{L} = \int_o^{H_2} (P_s - P_2(x))\,dx$$

$$\Sigma\frac{F_x}{L} = \frac{F_x}{L} = \int_o^{H_1} (P_s - P_1(y))\,dy + \int_{H_1}^{H_1+g} (P_s - P_o)\,dy$$

$$\Sigma\frac{M}{L} = \frac{M}{L} = \int_o^{H_2} (P_s - P_2(x))\,x\,dx + \int_o^{H_1} (P_1(y) - P_s)\,y\,dy + \int_{H_1}^{H_1+g} (P_o - P_s)\,y\,dy$$

Pressure profiles: $$P_1(y) = \left\{P_o^2 + \frac{(P_s^2 - P_o^2)}{H_1}(H_1 - y)\right\}^{1/2}$$

$$P_2(x) = \left\{P_o^2 + \frac{(P_s^2 - P_o^2)}{H_2}(H_2 - x)\right\}^{1/2}$$

Resultants:

$$\frac{F_y}{L} = \left(P_s - \frac{2}{3}\frac{(P_s^3 - P_o^3)}{(P_s^2 - P_o^2)}\right)H_2$$

$$\frac{F_x}{L} = \left(P_s - \frac{2}{3}\frac{(P_s^3 - P_o^3)}{(P_s^2 - P_o^2)}\right)H_1 + (P_s - P_o)g$$

$$\frac{M}{L} = \frac{P_s}{2}(H_2^2 - H_1^2) + \frac{2}{3}\frac{P_o^3}{(P_s^2 - P_o^2)}(H_2^2 - H_1^2) - \frac{4}{15}\frac{(P_s^5 - P_o^5)}{(P_s^2 - P_o^2)^2}(H_2^2 - H_1^2)$$

$$- \frac{(P_s - P_o)}{2}(2H_1 g + g^2)$$

Figure 11.—Wafer seal pressure induced loads.

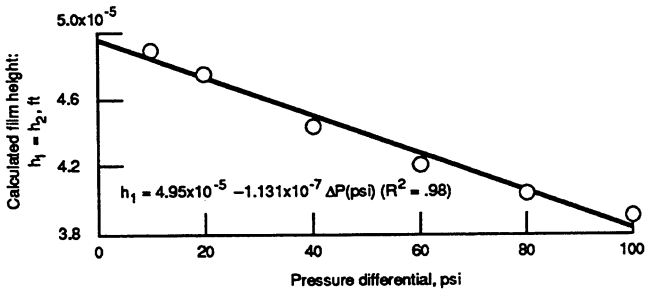

Figure 12.—Calculated film height versus simulated engine pressure differential.

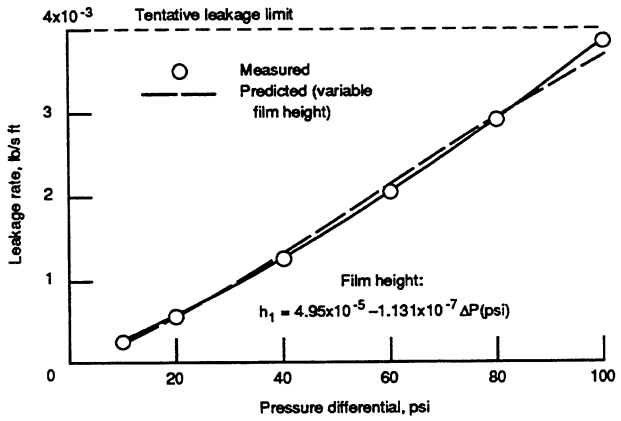

Figure 13.—Comparison of measured and predicted leakage rates versus simulated engine pressure differential using variable film height assumption.

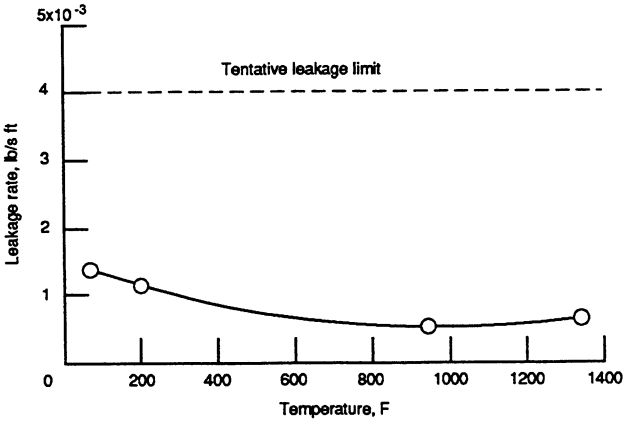

Figure 14.—Measured leakage rates as a function of temperature for a fixed engine pressure differential of 40 psi.

NASA
National Aeronautics and Space Administration

Report Documentation Page

1. Report No.	2. Government Accession No.	3. Recipient's Catalog No.
NASA TM -103737		

4. Title and Subtitle	5. Report Date
High Temperature Performance Evaluation of a Hypersonic Engine Ceramic Wafer Seal	April 1991
	6. Performing Organization Code

7. Author(s)	8. Performing Organization Report No.
Bruce M. Steinetz	E - 5942
	10. Work Unit No. 505 - 63 - 5B

9. Performing Organization Name and Address	11. Contract or Grant No.
National Aeronautics and Space Administration Lewis Research Center Cleveland, Ohio 44135 - 3191	
	13. Type of Report and Period Covered Technical Memorandum

12. Sponsoring Agency Name and Address	14. Sponsoring Agency Code
National Aeronautics and Space Administration Washington, D.C. 20546 - 0001	

15. Supplementary Notes

Responsible person, Bruce M. Steinetz, (216) 433 - 3302.

16. Abstract

Leakage rates of an innovative hypersonic engine seal have been measured using a specially developed static high temperature seal test fixture at NASA Lewis Research Center. The three foot long structural panel-edge seal is designed to minimize leakage of high temperature, high pressure gases past the movable panels of advanced ramjet/scramjet engines. The seal is made of a stack of precision machined ceramic wafer pieces that are inserted into a closely conforming seal channel in the movable engine panel. The wafer seal accommodates the significant distortions in the adjacent engine walls through relative sliding between adjacent wafers. Seal leakage rates are presented for engine simulated air temperatures up to 1350 °F and for engine pressures up to 100 psi. Leakage rates are also presented for the seal sealing both a flat wall condition, and an engine simulated distorted wall condition in which the distortion was 0.15 in. in only an 18 in. span. Seal leakage rates were low, meeting an industry-established tentative leakage limit for all combinations of temperature, pressure and wall conditions considered. Comparisons are made between the measured leakage rates and leakage rates predicted using a seal leakage model developed from externally-pressurized gas film bearing theory.

17. Key Words (Suggested by Author(s))	18. Distribution Statement
Seal; High temperature; Leakage modelling; Leakage rate measurement; Design	Unclassified - Unlimited Subject Category 37

19. Security Classif. (of the report)	20. Security Classif. (of this page)	21. No. of pages	22. Price*
Unclassified	Unclassified	24	A03

NASA FORM 1626 OCT 86

*For sale by the National Technical Information Service, Springfield, Virginia 22161

National Aeronautics and
Space Administration

Lewis Research Center
21000 Brookpark Rd.
Cleveland, OH 44135-3191